

## MIT Open Access Articles

*Photonic crystals: shaping the flow of thermal radiation*

The MIT Faculty has made this article openly available. **Please share** how this access benefits you. Your story matters.

**Citation:** Čelanović, Ivan et al. "Photonic Crystals: Shaping the Flow of Thermal Radiation." MRS Proceedings 1162 (2011)

**As Published:** <http://dx.doi.org/10.1557/PROC-1162-J01-02>

**Publisher:** Cambridge University Press

**Persistent URL:** <http://hdl.handle.net/1721.1/71635>

**Version:** Author's final manuscript: final author's manuscript post peer review, without publisher's formatting or copy editing

**Terms of use:** Creative Commons Attribution-Noncommercial-Share Alike 3.0



# Photonic Crystals: Shaping the Flow of Thermal Radiation

Ivan Čelanović, Michael Ghebrebrhan, Yi Xiang Yeng, John Kassakian, Marin Soljačić and John Joannopoulos  
Massachusetts Institute of Technology, 77 Massachusetts Ave., Cambridge, MA 02139

## ABSTRACT

In this paper we explore theory, design, and fabrication of photonic crystal (PhC) based selective thermal emitters. In particular, we focus on tailoring spectral and spatial properties by means of resonant enhancement in PhC's. Firstly, we explore narrow-band resonant thermal emission in photonic crystals exhibiting strong spectral and directional selectivity. We demonstrate two interesting designs based on resonant  $Q$ -matching: a vertical cavity enhanced resonant thermal emitter and 2D silicon PhC slab Fano-resonance based thermal emitter. Secondly, we examine the design of 2D tungsten PhC as a broad-band selective emitter. Indeed, based on the resonant cavity coupled resonant modes we demonstrate a highly selective, highly-spectrally efficient thermal emitter. We show that an emitter with a photonic cut-off anywhere from 1.8  $\mu\text{m}$  to 2.5  $\mu\text{m}$  can be designed.

## INTRODUCTION

The ability of photonic crystals to modify spontaneous emission and as a consequence, their ability to tailor thermal radiation has received significant attention in recent years [1,2]. It was shown that photonic crystals offer unparalleled possibilities for designing thermal radiation sources with properties that are often non-intuitive and deviate significantly from those of typical grey-body sources [3-10].

There are two general research areas being pursued with regard to shaping thermal radiation using photonic crystals. On the one hand, photonic crystals are used to design highly selective narrow-band thermal emitters, exhibiting wavelength, directional and polarization selectivity. These structures show promise for applications in IR sensors and a variety of IR sources[3-7]. On the other hand, PhC's are explored to design wide-band, selective thermal emitters exhibiting near blackbody thermal emission within a given wavelength range and largely attenuated emission outside the given range [8-10]. Applications such as thermophotovoltaic energy conversion, solar-thermophotovoltaic conversion, and solar absorbers/reflectors are considered as main drivers behind advances in broad-band selective thermal emitters.

In the following sections we will explore the opportunities that electromagnetic resonances in PhC's present for tailoring thermal radiation properties. We will start our exploration with a simple one-dimensional (1D) PhC structure that can be designed to exhibit narrow-band emittance. In addition, we will examine how almost totally transparent thin silicon PhC slab can be designed to exhibit narrow-band resonant thermal emission. Lastly, we will address how a broad-band thermal emitter can be designed based on multiple electromagnetic resonances.

## NARROWBAND RESONANT THERMAL EMISSION

Bulk thermal emission sources are commonly perceived as isotropic, broad-band and incoherent electromagnetic radiation sources. We will show that based on resonant Q-matching in 1D and 2D periodic structures narrow-band quasi-coherent thermal radiation sources can be designed.

### Vertical cavity enhanced resonant thermal emission (VERTE)

Our design for vertical cavity resonant thermal emission (VERTE) was inspired by the vertical cavity surface emitting laser (VCSEL) [5]. However, unlike the VCSEL, where the active medium is embedded in the cavity between the two 1D PhC's, the VERTE consists of a cavity sandwiched between a partially reflective 1D PhC on one side and a highly reflective metallic mirror on the other side, as shown in figure 1. Ideally, the 1D PhC and the cavity are lossless (i.e. they are highly transparent in the range of wavelengths that are of interest) while the metallic mirror is highly reflective yet slightly absorbing—thus acting as both the high-temperature source of radiation and the cavity mirror. The cavity, with its strong frequency dependent transfer function, enhances thermal emission originating from the metallic mirror, building up a strong quasi-monochromatic field while suppressing non-resonant frequencies.

The schematics of the VERTE structure is given in figure 1. The structure consists of high-reflectance (low-absorption) metallic layer, a cavity (a dielectric cavity layer), and a 1D PhC. In the ideal case, metallic mirror acts as both cavity mirror and as a source of thermal radiation, assuming that all the other layers are lossless. The photonic crystal on the other side of the cavity acts as partially reflective mirror. Typical normal emittance of a VERTE structure is given in figure 2 and compared to the emittance of the flat silver layer. Large narrow-band emittance enhancement is due to resonant cavity enhancement effect [5].

To model the emittance of VERTE we will use Kirchoff's law, stating that emittance and absorptance are equivalent. We derive the reflectance using temporal coupled mode theory, an extremely powerful analytical tool that provides very interesting insights into the design trade-offs and performance. Detailed derivation of coupled mode theory is given in [11]. Resonant mode amplitude is given as:

$$\frac{d}{dt} a_m = -j\omega_0 a_m - \left( \frac{1}{\tau_{int}} + \frac{1}{\tau_{ext}} \right) a_m + \sqrt{\frac{2}{\tau_{ext}}} s_+ \quad (1)$$

where  $a_m$  is the resonant mode amplitude,  $\omega_0$  is the resonant frequency,  $\tau_{int}$  is the internal cavity mode decay rate (due to internal dissipative losses),  $\tau_{ext}$  is the external decay rate due to the power leaking from the resonator, and  $s_+$  is the incoming wave amplitude that is feeding the resonator externally. It can be shown that the absorptance can be expressed as:

$$|A|^2 = 1 - |R|^2 = \frac{4}{(\omega - \omega_0)^2 + \left( \frac{1}{\tau_{int}} + \frac{1}{\tau_{ext}} \right)^2}, \quad (2)$$

where  $|A|^2$  is the absorptance and  $|R|^2$  is the reflectance. From this equation it is immediately obvious that in order to maximize the emittance at the resonance one needs to match internal and external decay rates. In other words internal and external cavity  $Q$ 's had to be equal.

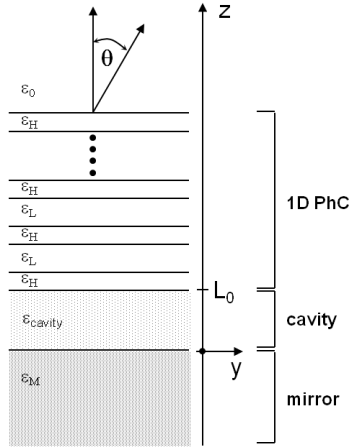


**Figure 1.** Cross-sectional view of vertical-cavity enhanced resonant thermal emitter (VERTE).

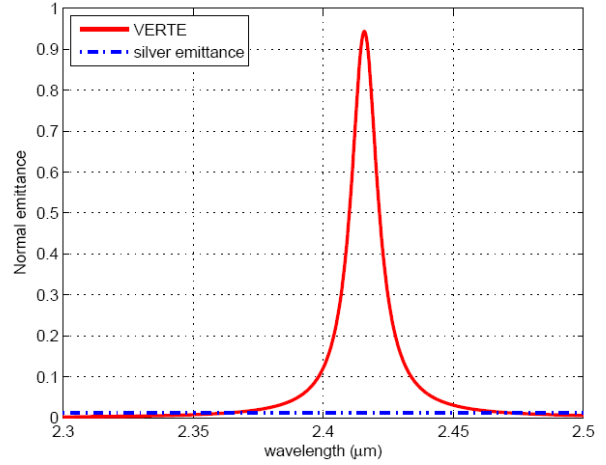


**Figure 2.** Normal emittance of vertical-cavity enhanced resonant thermal emitter with silver and normal emittance of planar silver

In addition, for this 1D case all parameters of the cavity  $\tau_{int}$ ,  $\tau_{ext}$ , and  $\omega_0$  can be calculated analytically. This enables us to tune resonant wavelength, adjust  $\tau_{ext}$  by changing the number of PhC layers and thus changing the rate of out-coupling so that it matches with the internal cavity losses. By changing the losses in the material, or by using different materials it is possible to design different narrow-band emitters operating in different wavelength ranges and exhibiting different full-width at half maximums. This approach also enables tailoring of directional radiation properties.

### **Fano-resonance enhanced thermal emission in 2D PhC slab**

A PhC slab with a 2D-periodic array of holes gives rise to a number of Fano-resonances [12]. It was shown that using these leaky resonances, for example in silicon (Si) PhC slabs, multiple narrow-band resonant emission peaks in the infrared regime, reaching a peak emittance of 50% at the resonant wavelength compared to virtually 0% emittance of plain Si slabs can be obtained. This huge increase can be achieved via resonant  $Q$ -matching, whereby the quality factor ( $Q$ ) of the Fano resonances is matched to the  $Q$  of the internal losses. In principle, this is similar to the VERTE approach.

Without patterning (i.e. regular silicon slab), the transmittance follows the standard quarter wave behavior, where maximum transmission occurs whenever the slab fits a multiple of half a wavelength. Upon introduction of a square lattice of holes, two sharply peaked resonances are observed. The introduction of periodicity allowed coupling of external waves to guided resonances which exhibit strongly confined fields in regions of higher dielectric. Due to the leaky nature and coupling to the external environment of this type of resonance, coupled mode theory is again extremely useful modeling tool. For two resonances of different parity with

respect to the horizontal mirror plane, the transmission coefficient of the patterned slab,  $t_{PhC}$ , is given as [6]:

$$t_{PhC} = t_{slab} - \frac{(t_{slab} + r_{slab}) \frac{1}{\tau_1}}{j(\omega - \omega_1) + \frac{1}{\tau_1}} - \frac{(t_{slab} - r_{slab}) \frac{1}{\tau_2}}{j(\omega - \omega_2) + \frac{1}{\tau_2}} \quad (3)$$

where  $t_{slab}$  and  $r_{slab}$  is the transmission and reflection coefficient of a plain Si slab,  $\omega_1$  and  $\omega_2$  are resonant frequencies of the first and second mode, and  $\tau_1$  and  $\tau_2$  are the lifetime of the modes respectively. As shown in figure 4, the coupled mode theory model agrees well with numerical simulation.

In practice, free standing slabs of sub-micron thicknesses are difficult to fabricate as they are susceptible to fracture due to high sheer and bending stresses. Hence, it is preferable to fabricate these structures on top of a substrate. A suitable substrate is sapphire due to its ultra low absorption in the infrared wavelength regime. Since sapphire has a refractive index close to  $n=1.7$  (significantly below silicon), we expect the behavior to be very similar to the free standing slab. This is confirmed by a field profile that shows confinement of fields that is almost exact to the free-standing slab case as shown in figure 5. Nevertheless, the addition of sapphire causes a significant change in the resonant frequency as shown in figure 6. This is expected due to the variational theorem, whereby lower eigen frequencies result when fields are confined in higher dielectric substances. However, this is not a problem as we can tailor both the periodicity  $a$ , and the radius  $r$  of the holes to obtain the required resonant frequency as shown in figure 7. As the radius is increased, the resonant frequency increases while  $Q$  decreases.

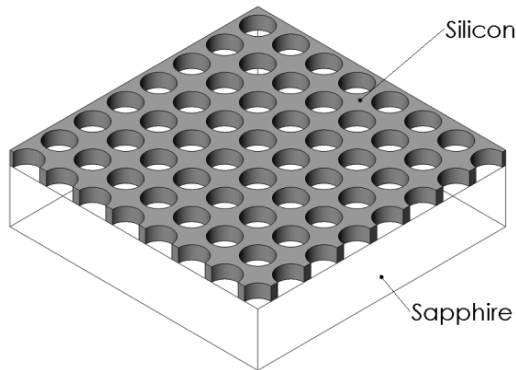


**Figure 3.** Si PhC slab of thickness  $t$  with holes of radius  $r$  and period  $a$  in a square lattice on top of a sapphire substrate.

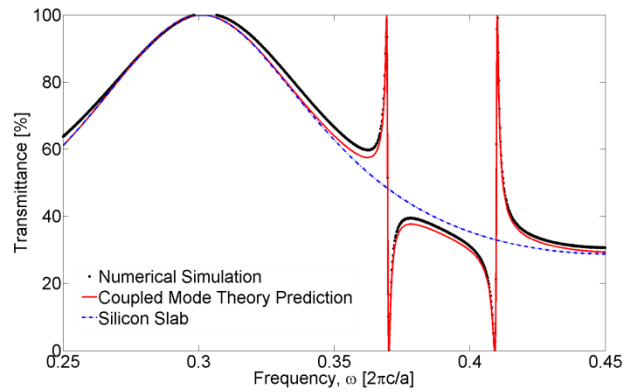


**Figure 4.** Transmittance of free standing Si PhC with  $r = 0.20a$  and  $t=0.5a$  at normal incidence. As can be seen, coupled mode theory agrees well with numerical simulation. The first two resonances are exhibited here.

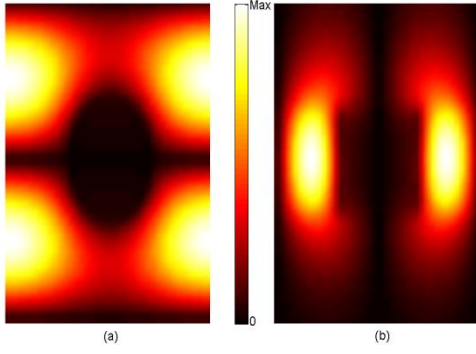


**Figure 5.** Magnitude of  $H_z$  in Silicon on Sapphire structure for (a) Horizontal Slice (b) Vertical Slice. The fields are strongly confined in areas of higher dielectric.

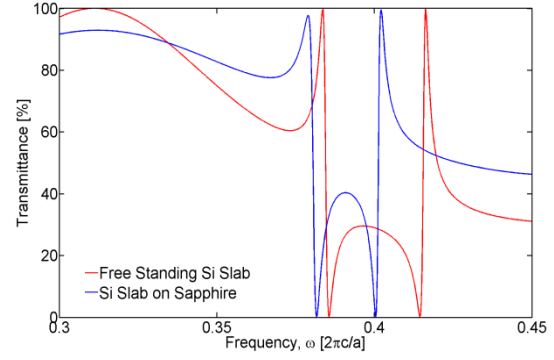


**Figure 6.** Transmittance plots obtained from numerical simulation for free standing Si slab and Si Slab on sapphire. All Si slabs have radius of  $r = 0.20a$ .

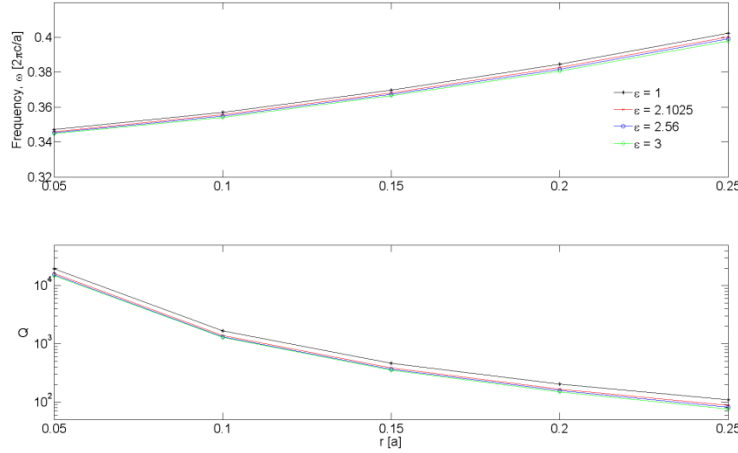


**Figure 7.** Plots of resonant frequency and resonance quality factor  $Q$  at normal incidence for first odd mode as a function of hole radius.

Next, we proceed with adding absorption losses in our model, as absorptance is necessary for emission. The absorption is included by adding an additional decay route in coupled mode theory. In practice, absorption can be introduced by doping silicon slab to control conductivity or by injecting free carriers. Since the field profile is almost exactly the same and the interaction time similar compared to the free standing Si slab, it is reasonable to model the asymmetrical case of silicon on sapphire with the same coupled mode equations derived for the symmetrical free standing case given in (3). The modified transmission coefficient, reflection coefficient, and absorption are then given by the following expressions:

$$t_{PhC} = t_{slab} - \frac{(t_{slab} + r_{slab}) \frac{1}{\tau_1}}{j(\omega - \omega_1) + \frac{1}{\tau_1} + \frac{1}{\tau_{int}}} - \frac{(t_{slab} - r_{slab}) \frac{1}{\tau_2}}{j(\omega - \omega_2) + \frac{1}{\tau_2} + \frac{1}{\tau_{int}}} \quad (4)$$

$$r_{PhC} = r_{slab} - \frac{(t_{slab} + r_{slab}) \frac{1}{\tau_1}}{j(\omega - \omega_1) + \frac{1}{\tau_1} + \frac{1}{\tau_{int}}} + \frac{(t_{slab} - r_{slab}) \frac{1}{\tau_2}}{j(\omega - \omega_2) + \frac{1}{\tau_2} + \frac{1}{\tau_{int}}} \quad (5)$$

$$|A|^2 = 1 - |r_{PhC}|^2 - |t_{PhC}|^2 = \frac{\frac{2}{\tau_1 \tau_{1int}}}{(\omega - \omega_1)^2 + (\frac{1}{\tau_1} + \frac{1}{\tau_{1int}})^2} + \frac{\frac{2}{\tau_2 \tau_{2int}}}{(\omega - \omega_2)^2 + (\frac{1}{\tau_2} + \frac{1}{\tau_{2int}})^2} \quad (6)$$

where  $|A|^2$  is the absorption coefficient of the patterned slab and  $\tau_{1int}$  is the lifetime associated with the internal conduction losses of the first resonance and  $\tau_{2int}$  is the lifetime associated with the internal conduction losses of the second resonance. Indeed, equation (6) is very similar to (2) and reveals the same physical concepts involved in resonant  $Q$  matching although the structures are very different

The results of coupled mode theory analysis when the  $Q$ 's are matched are shown in figure 8. Emittance is seen to strongly peak at the resonant frequencies. Physically, the enhancement of emission at the resonances is due to the longer interaction time with the lossy material due to the strongly confined nature of the resonances. In contrast, plain Si slabs do not allow coupling into such modes, thereby only allowing light to transmit unimpeded, resulting in a short interaction time. This demonstration provides a viable path towards producing narrow-band thermal emitters that can be easily tuned through current micro-fabrication technologies.

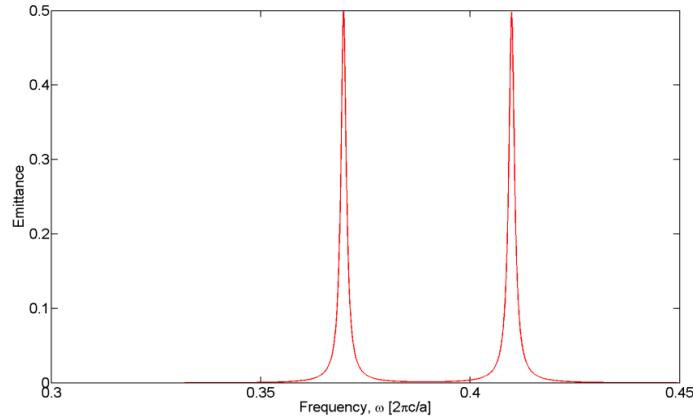


**Figure 8.** The absorption peaks to a maximum of 50% at the resonance frequencies when the internal and external  $Q$ 's are matched.

## RESONANTLY ENHANCED BROADBAND THERMAL EMISSION

We can now switch gears and shift our attention to the two-dimensional tungsten photonic crystal consisting of square array of deep cylindrical holes, designed as a broadband thermal emission source.

Similar results can be obtained with different types of lattice (e.g. hexagonal) and different cavity shapes (e.g. square), yet we have adopted the square lattice and cylindrical holes due to easier micro-fabrication and potential for scalability. Several groups reported studies of similar 2D tungsten periodic structures designed to enhance thermal emission. In [8], the authors reported on a microstructured tungsten emitter (that consists of a square array of posts) with relatively small aspect ratio fabricated in sputtered tungsten. In [9], a 2D tungsten grating consisting of a periodic array of square cavities, fabricated using electron beam lithography and fast ion beam etching in both single crystal and polycrystalline tungsten, was reported.

Here we focus on a 2D W PhC that consists of a square array of deep cylindrical cavities with fixed period  $a=1\text{ }\mu\text{m}$ , and different cavity radii  $r$  and depths  $d$  are studied [13]. In the design process we rely on enhancing thermal emission over a relatively broad wavelength range by the mechanism of coupling resonant cavity electromagnetic modes. This enables us to design a wide-bandwidth thermal radiation source with very weak angular and polarization dependence.

Simulation and experimental results for normal emittance of flat tungsten and three different 2D tungsten PhC geometries are given in figure 9. For simulation purposes we used tungsten optical properties that are given in [14]. All simulated PhC's exhibit large resonantly enhanced emittance peaks, which are directly related to the cylindrical cavity cutoff mode. The first resonant emission peaks, shown in figure 9, correspond to the lowest order transverse electric (TE) resonant mode of the cylindrical cavity.

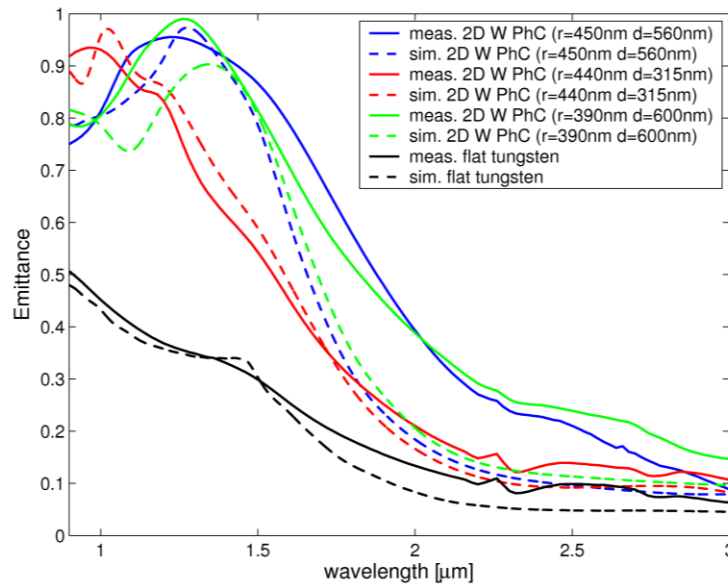


**Figure 9.** Measured and simulated normal emittance for flat tungsten and three 2D W PhC.

### **Micro-fabrication process**

The fabrication process consists of two major parts: lithography and etching. The sample pattern was produced using laser interference lithography, a technique that enables fast, large-scale fabrication of a variety of micro- and nano-scale patterns. The pattern is then transferred into the underlying tungsten substrate by etching. The fabrication process steps are illustrated in figure 10. The chromium (Cr) "hard-mask" layer is deposited using electron-beam evaporation. The two lithography layers - anti-reflective coating (ARC) and photoresist (PR) - are applied



using a spinning stage. The photoresist layer captures the lithographic pattern, while the ARC acts as a feature-enhancing role. The principle behind the laser interference lithography technique is that of the interference of two coherent light beams. Using a laser source and a mirror, a variety of interference patterns is created by changing the angle between the mirror and the sample. The mirror angle determines the period of the structure, while the duration of exposure determines the cavity radius. After lithography, the pattern is developed using a commercial photoresist developer. Oxygen-based reactive ion etching (RIE) is used to transfer the pattern from the photoresist into the ARC layer. The chromium wet etch process transfers the pattern from the ARC layer into the chromium hard-mask layer. Using diluted chromium etchant facilitates control of the cavity radius, a critical dimension in our structure. Having served its purpose, the remaining ARC was removed using the same RIE oxygen-based recipe. The final etch step is a carbon-tetrafluoride-based tungsten RIE. The depth to which tungsten can be etched is limited by the thickness of the chromium mask. The chromium mask is initially very durable, but slowly erodes during the tungsten RIE. Complete destruction of the chromium layer leads to poor top-surface quality of the final tungsten structure. In our particular case, 50 nm of chromium lasted until a depth of approximately 600 nm is etched in the tungsten.

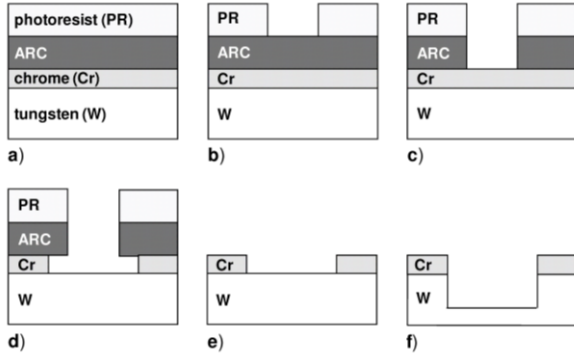


**Figure 10.** Flowchart of the 2D W PhC microfabrication process.

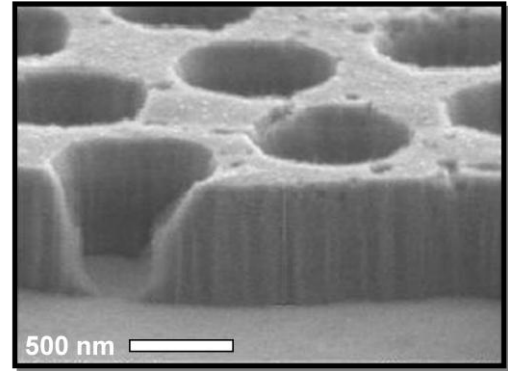


**Figure 11.** SEM image of fabricated 2D single crystal tungsten PhC sample with the following parameters: radius  $r=390$  nm, whole depth  $d=600$  nm, and period  $a=1$   $\mu\text{m}$ .

## CONCLUSIONS

In conclusion we have demonstrated that electromagnetic resonances in photonic crystals present an extremely powerful and versatile tool for tailoring thermal emission properties. We have shown only certain aspects of tailoring and tuning thermal radiation, yet many more properties remain largely unexplored such as temporal and spatial coherence properties, near field energy distribution and non-equilibrium temperature distribution to name a few.

Incredible advancements in terms of photonic crystal theory, design and fabrications in the last decade had enabled what many thought was impossible in terms of shaping thermal emission. These new developments are in turn enabling new and more efficient static energy conversion devices and sensors, ranging from thermophotovoltaics, solar-thermophotovoltaics, solar-thermal and infrared sensors to name a few. The unprecedented level of control over thermal radiation that photonic crystals enable will only continue to fuel the research and find new applications.

## ACKNOWLEDGMENTS

This research was supported in part by the U.S. Army Research Office through the Institute for Soldier Nanotechnologies and The Sheila and Emmanuel Landsman Fellowship.

## REFERENCES

1. E. Yablonovitch, *Phys. Rev. Lett.* **58**, 2059 (1987)
2. S. John, *Phys. Rev. Lett.* **58**, 2486 (1987).
3. J. J. Greffet, R. Carminati, K. Joulain, J. P. Mulet, S. Mainguy, and Y. Chen, *Nature* (London) **416**, 61, 2002.
4. M. U. Pralle, N. Moelders, M. P. McNeal, I. Puscasu, A. C. Greenwald, J. T. Daly, E. A. Johnson, T. George, D. S. Choi, I. El-Kady, and R. Biswas, *Appl. Phys. Lett.* **81**, 4685 (2002).
5. I. Celanovic, D. Perreault, and J. Kassakian, *Phys. Rev. B* **72**, 075127 (2005).
6. D. L. C. Chan, I. Celanovic, J. D. Joannopoulos, and M. Soljačić, *Phys. Rev. A* **74**, 064901 (2006).
7. C. M. Cornelius and J. P. Dowling, *Phys. Rev. A* **59**, 4736 (1999).
8. A. Heinzl, V. Boerner, A. Gombert, B. Blasi, V. Wittwer, and J. Luther, *J. Mod. Opt.* **47**, 2399 (2000).
9. H. Sai, Y. Kanamori, and H. Yugami, *Appl. Phys. Lett.* **82**, 1685 (2003).
10. J. G. Fleming, S. Y. Lin, I. El-Kady, R. Biswas, and K. M. Ho, *Nature* (London) **417**, 52 (2002).
11. H. A. Haus, *Waves and Fields in Optoelectronics*, Prentice-Hall, Englewood Cliffs, NJ, (1984).
12. S. Fan and J. D. Joannopoulos, *Phys. Rev. B* **65**, 235112 (2002).
13. I. Celanovic, N. Jovanovic, and J. Kassakian, *Appl. Phys. Lett.* **92**, 193101 (2008).
14. E. D. Palik, *Handbook of Optical Constants of Solids* \_Academic, Orlando (1985).